CrystEngComm

RSC Publishing

PAPER

View Article Online
View Journal | View Issue

Structural investigation of Li_2O–B_2O_3–MoO_3 glasses and high-temperature solutions: toward understanding the mechanism of flux-induced growth of lithium triborate crystal

Cite this: *CrystEngComm*, 2013, **15**, 356

Di Wang,* Ji Zhang, Deming Zhang, Songming Wan, Qingli Zhang, Dunlu Sun and Shaotang Yin

MoO_3 is an important flux for lithium triborate (LiB_3O_5) crystal growth from high-temperature solutions. Although it has been widely used, the mechanism of the MoO_3 flux-induced growth of LiB_3O_5 crystals is still not very clear. In this paper, we present a spectroscopic investigation of the Li_2O–B_2O_3–MoO_3 ternary glasses/solutions, which were prepared from high-temperature MoO_3-based solutions for LiB_3O_5 crystal growth. By combining all the experimental data of Raman and MAS NMR, the types of structural species and the interactions between flux and solute are discussed to understand the MoO_3 flux-reduced mechanism of LiB_3O_5 crystallization from the high-temperature solution. Considering the activities of lithium cations, an isomerization reaction is proposed to describe the structural evolution of the $B\emptyset_4$ tetrahedron into the $B\emptyset_3$ triangle in boroxol due to the MoO_3 flux. The transition between the boron oxide species is essential for the LiB_3O_5 crystal growth. On cooling, the formed boroxol rings are polymerized by the re-formation of $B\emptyset_4$ tetrahedrons again, and gather together to form the LiB_3O_5 crystal phase. Finally, the MoO_3 flux-induced LiB_3O_5 crystallization may be elucidated with the decrease of the concentration of the $B\emptyset_4$ tetrahedron in high-temperature solutions.

Received 1st August 2012,
Accepted 25th October 2012

DOI: 10.1039/c2ce26231b

www.rsc.org/crystengcomm

Introduction

Lithium triborate, LiB_3O_5 (LBO), is an excellent functional crystal used in non-linear optics (NLO) for laser radiation in the visible and ultraviolet regions.[1,2] Because the LBO crystal melts incongruently at 834 $\pm$ 4 °C, the bulk single crystal can be grown only by the high-temperature solution growth technique. The B_2O_3 self-flux or the MoO_3-based flux systems are considered to be the best choice for LBO crystal growth. The former could efficiently avoid the incorporation of heterogeneous ions into the grown crystal, but have a high inherent solution viscosity, due to a large amount of B_2O_3 (>90 wt%) which limits the crystallization range for the high quality LBO crystal growth.[3,4] Compared with the B_2O_3 self-flux, the MoO_3-based flux has a low viscosity and a high solubility for LBO, which allows for a significant improvement in both size and quality of the grown LBO crystal. The growth of the LBO crystal using the MoO_3 flux has been intensely investigated by many researchers.[5–10] Parfeniuk *et al.*[5,6] reported a pseudo-binary phase diagram of the $Li_2O{\cdot}3B_2O_3$–MoO_3 system for the first time; Pylneva *et al.*[7] investigated the Li_2O–B_2O_3–MoO_3 ternary system in detail, and suggested the crystallization region for the LBO growth. Recently, Kokh *et al.*[8] reported the growth of a LBO crystal of more than 1.3 kg using the technology of heat field symmetry control; Hu *et al.*[9] and Nikolov *et al.*[10] improved the crystal weight to 2.0 kg under optimized growth conditions, respectively. However, these previous studies focused mainly on the crystal growth technologies, and the fundamental mechanism of the flux-induced growth of the LBO crystal is still not well understood.

Our previous studies of the growth mechanism of borate crystals have proved that structural information of the high-temperature melt/solution is important for understanding the kinetic processes of crystal growth at a molecular level.[11–15] For instance, an *in situ* Raman investigation of the LBO growth from the B_2O_3 self-flux solution[11] revealed that the cyclic boron oxide species of the $Li_2O{\cdot}4B_2O_3$ solution (the excess B_2O_3 as the self-flux) were similar to that of the LBO crystal. The cyclic species in the $Li_2O{\cdot}4B_2O_3$ solution were called "crystal growth units", which were composed of three-coordinated boron $B\emptyset_3$ (Ø represents a bridging oxygen) and four-coordinated boron $B\emptyset_4$. Moreover, the conversion between the $B\emptyset_3$ and $B\emptyset_4$ was closely related to the growth and melting of LBO crystals. For a congruent CsB_3O_5 (CBO) crystal growth, a similar dynamic process was also found and

Anhui Institute of Optics and Fine Mechanics, Chinese Academy of Sciences, Hefei 230031, China. E-mail: wangdiean@gmail.com; Fax: +86 0551 5591039; Tel: +86 0551 5591039

applied to explain the observed growth habit of the CBO crystal very well.[12,13]

Unfortunately, the structural investigation on the high-temperature melt/solution is still an experimental challenge due to the extreme conditions (high temperatures, high volatility). Glasses are described as the frozen image of the high-temperature liquid at a certain "fictive temperature" (T_f), whose structures could be studied conveniently and precisely at ambient temperature.[16] The alkali borate melt is a typical glass-forming liquid due to the highly cross-linked boron oxide network.[17] The structural characteristics of the alkali-borate glasses are the various cyclic boron oxide species, which are polymerized by $BØ_3$ planar triangles and $BØ_4$ tetrahedrons, and alkali ions act as the network modifier balancing the charge and modifying structures of the glasses. Raman and magic-angle-spinning nuclear magnetic resonance (MAS NMR) spectra have been proven to be powerful and simple methods for structural determination in borate compounds.[18–24] The sharp Raman vibration peaks could suggest the species of boron oxide species and molybdenum oxide species in glasses/melts;[18–20] ^{11}B MAS NMR could clearly separate the $BØ_4$ and $BØ_3$ peaks and accurately estimate their relative concentrations in glasses. Moreover, ^{7}Li MAS NMR could potentially provide the environmental information of Li ions.[21–24]

In this paper, the structures of the Li_2O–B_2O_3–MoO_3 glasses and high-temperature solutions were investigated using Raman and ^{11}B, ^{7}Li MAS NMR spectra. Basing on the structural interpretation of the high-temperature solutions, the interaction between the flux (MoO_3) and the solute (LBO compound) were discussed, and the mechanism of flux-induced growth of the LBO crystal could be proposed. The results indicated that LBO crystallization from the high-temperature solution might be closely correlated to the reduction of $BØ_4$ tetrahedrons in solutions due to the MoO_3 flux.

Experimental section

Samples preparation

Reagent grade lithium carbonate, boric acid and molybdenum oxide were used for the preparation of seven samples, whose compositions lied in the crystallization region of Li_2O–B_2O_3–MoO_3 phase diagram (Fig. 1). The nominal compositions of these samples were given in Table 1. The well-mixed starting materials were melted in a pure Pt crucible at a temperature 50 K above the crystallization point (depending on the compositions). The high-temperature liquid was heated for at least 24 h with vigorous machine stirring to ensure homogenization and fining. The glassy samples were obtained by rapidly quenching the melts in liquid nitrogen. X-ray diffraction data were applied to check the amorphous state of glasses, and revealed MoO_3 crystalline impurities existed in these glasses with the high molybdenum oxide contents (LBM5, LBM6). The negligible weight loss of each sample indicated the composition was close to nominal.

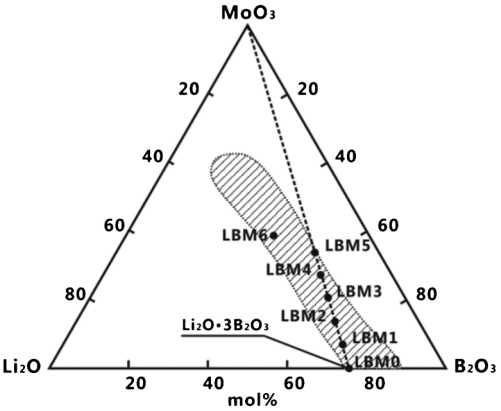

Fig. 1 Seven samples are indicated in the Li_2O–B_2O_3–MoO_3 ternary phase diagram. The shadow area is the crystallization region suggested by Parfeniuk *et al.*,[7] and the dashed line is the $Li_2O{\cdot}3B_2O_3$–MoO_3 binary system.

Raman spectroscopy

Unpolarized Raman spectra of glasses and solutions were obtained using a Jobin Y'von U1000 laser Raman spectrometer with the 514.5 nm line of an Ar^+ laser as the excitation source. Laser at power levels of 30 mW for room temperature spectra and 60 mW for high-temperature spectra was focused on the sample using an Olympus BH-2 microscope. The Raman scattering light from the sample was collected by a back-scattering confocal lens system, and detected by a charge-coupled device (CCD). During the scattering integration time of 10 s, Raman spectra over a wide frequency range of 100–1800 cm^{-1} were obtained with the spectral resolution better than 2 cm^{-1}.

In order to measure Raman spectra of the high-temperature solution, the corresponding glassy samples in a size of 12 mm × 7 mm × 2 mm were melted by a homemade electronic microfurnace, which was coupled with the Raman spectrometer. The melts were held at measuring temperature for several minutes before spectra collection. The experimental parameters were consistent with those at room temperature except the laser power. Due to the blackbody radiation at high temperature, the highest measuring temperature was limited

Table 1 Sample names and nominal compositions

Sample name	Mole fraction[a] $Li_2O : B_2O_3 : MoO_3$	T_c[b] (°C)
LBM0	1 : 3 : 0	834[c]
LBM1	1 : 3 : 0.2	780
LBM2	1 : 3 : 0.4	750
LBM3	1 : 3 : 0.8	722
LBM4	1 : 3 : 1.2	700
LBM5	1 : 3 : 1.7	660
LBM6	2 : 3 : 3	730

[a] For LBM0–5, the weight fractions of MoO_3 were 0, 10, 20, 30, 40 and 50 wt%, respectively. [b] The crystallization temperature of LBO from high-temperature solutions except LBM0. [c] The incongruent melting temperature of $Li_2O{\cdot}3B_2O_3$ compound, but $Li_2B_4O_7$ crystal precipitates.

to about 1000 °C. For all spectra, the intensities were corrected for background and the Bose–Einstein population reduced factor, then fitted using Gaussian-type profile by the least square method for obtaining the peak elements, such as peak position, shape and area. The initial variables of elements were referenced on the previous publications about borate and molybdate glasses.

MAS NMR spectroscopy

MAS NMR spectra of the glassy samples (LBM0–4) were recorded on a Bruker Avance 400 spectrometer with a 4 mm Bruker MAS probe. The Larmor frequencies were at 128.38 MHz for ^{11}B and 155 MHz for ^{7}Li, respectively. The ^{11}B and ^{7}Li chemical shifts were given in parts per million (ppm) with respect to the BF3.O (CH_2CH_3) standard relative to 1.0 M boric acid at −19.6 ppm and the 9.7 M LiCl aqueous solution at 0.0 ppm. Si_3N_4 and ZrO_2 rotors hold the ground glassy powders, rotated at a speed of 15 kHz for ^{11}B and 17 kHz for ^{7}Li. In order to determine the relative amount of various boron oxide species in glasses quantitatively, ^{11}B MAS spectra were collected using a short hard pulse width 0.265 μs with a recycle delay of 2 s at a frequency of 70 kHz. Decomposition and integration of these spectra were performed using the Dmfit program[25] with proper Gaussian–Lorentzian line shapes.

Results

Raman spectra of Li_2O–B_2O_3–MoO_3 glasses

Due to high bond valence with oxygen, molybdenum ions have a lower solubility in borate glasses, thus molybdates readily crystallize out on cooling. In this work, the pure vitreous state without crystallization could be obtained from LBM0–4 samples. Raman spectra of these glasses in the range of 100–1100 cm^{-1} were recorded at room temperature (Fig. 2). For the LBM0 glass containing no MoO_3, the strongest Raman peak was at 783 cm^{-1}. Considering the bands at 510, 655 and 953 cm^{-1}, the 783 cm^{-1} peak was attributed to the breathing vibration of the boron oxide ring containing one $BØ_4$ tetrahedron,[18–20,26] *i.e.* one $B_3Ø_7$ ring composed of two $BØ_3$ units and one $BØ_4$ unit. Besides the Raman peak at 783 cm^{-1}, another weak peak was observed at 808 cm^{-1}. This peak was considered to be the well-known characteristic of vitreous B_2O_3, which originated from the breathing vibration of the boroxol ring,[27] *i.e.* one $B_3Ø_6$ ring composed of three $BØ_3$ units without $BØ_4$ units. However, the 808 cm^{-1} peak was very weak, and the 783 cm^{-1} peak was the uniquely predominant feature of the LBM0 spectrum (Fig. 2).

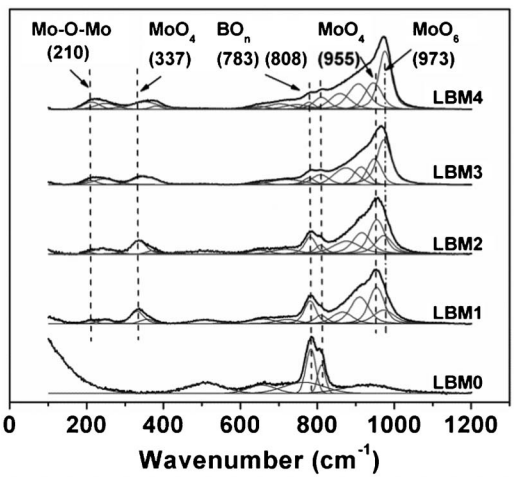

Fig. 2 Experimental Raman spectra and the fitting results of LBM0–4 borate glasses.

For the glasses containing MoO_3, Raman peaks could be divided into two categories: (a) the ones around 700–800 cm^{-1} were ascribed to the vibrations of the cyclic boron oxide species with or without $BØ_4$ units;[18–20,26,27] (b) the others around 850–980 cm^{-1} and 200–400 cm^{-1} were ascribed to the vibrations of molybdenum oxide species, such as the MoO_4 tetrahedron and the MoO_6 octahedron.[28–31] The LBM1 glass with 10 wt% MoO_3 had two dominant peaks at 955 and 861 cm^{-1}, which were accompanied with a weak peak at 337 cm^{-1} (Fig. 2). As the assignment in previous works,[28,29] two high-frequency peaks were ascribed to the symmetric and asymmetric stretching vibrations of isolated MoO_4 tetrahedrons in glass, and the low-frequency peak was ascribed to bending vibration of Mo–O bonds in these MoO_4 tetrahedrons. Another weak vibration peak was found at 973 cm^{-1} and ascribed to stretching vibration of Mo=O bonds in distorted MoO_6 octahedrons.[28–32] The lower intensity of the peak at 973 cm^{-1} compared to 955 cm^{-1} indicated that in borate glasses with low MoO_3 content, molybdenum ions preferred to locate at tetrahedral sites in form of MoO_4 units. As the MoO_3 content increased, a gradual increase in strength of 973 cm^{-1} occurred. For the glasses containing more than 30 wt% MoO_3, the 973 cm^{-1} peak became stronger than the 955 cm^{-1} peak. The intensity enhancing of the 973 cm^{-1} peak suggested MoO_6 octahedrons in glasses increased along with the increase of MoO_3. Additionally, the low-frequency peak observed at 210 cm^{-1} was ascribed to bending vibration of Mo–O–Mo bonds in MoO_6 octahedrons,[28–32] and indicated the MoO_6 octahedrons were linked together by sharing oxygen corners. On the other hand, the positions of Raman peaks ascribed to boron oxide rings were not affected by the addition of MoO_3, and still appeared at 781 and 810 cm^{-1}. When the MoO_3 content increased gradually, the relative intensity of 781 cm^{-1} to 810 cm^{-1} experienced a downward trend, which suggested a proportional reduction of $BØ_4$ tetrahedrons in glasses.

Because no Raman peak attributed to vibrations of molybdenum oxide species appears in the high-frequency region, the broad-band of 1200–1600 cm^{-1} (Fig. 3) is only associated to the stretching vibration of the B–O bonds in various boron oxide triangles. The previous studies of low-alkali borate glasses have suggested these triangles: (a) the symmetric $BØ_3$ units in boroxol rings or being part of a connected boron oxide network were attributed to P_1 around 1210–1260 cm^{-1} and P_2 around 1320–1370 cm^{-1};[20,27] (b) the BO_3 units linking to $BØ_4$ tetrahedrons were attributed to P_3 around 1500 cm^{-1};[33] (c) the asymmetric $BØ_2O^-$ units with non-bridge oxygen (NBO) or the $BØ_3$ units correlating with boroxol rings were both attributed to P_4 around 1530–1550

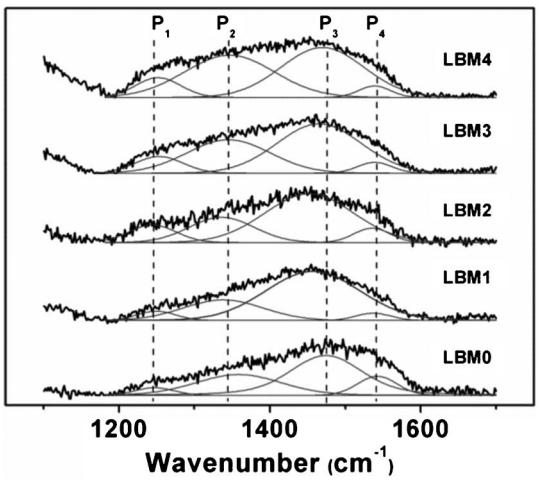

Fig. 3 Experimental Raman spectra and the deconvoluted results of the high-frequency band for LBM0–4 borate glasses. The four components labeled as P_{1-4} are discussed in the text.

cm^{-1}.[34] For LBM0–4 glasses, a multicomponent deconvolution of the broad-band was carried out based on four bands P_{1-4} (Fig. 3), the peak parameters of which were obtained (Table 2). For LBM0 glass, the primary component of the broad-band was the P_3 band around 1465–1475 cm^{-1}, which was ascribed to the BO_3 units linking to $BØ_4$ tetrahedrons. The addition of MoO_3 into borate glasses resulted in the P_3 band decreasing, conversely, three other weak bands increased. Especially for the P_2 band around 1350 cm^{-1}, the enhanced intensity of which suggested the formation of $BØ_3$ triangles along with the decrease of $BØ_4$ tetrahedrons in glass, and the broad FWHM suggested these $BØ_3$ units preferred to be the relatively disordered boroxol rings rather than the well-defined network former.

Due to the similar vibration mode, the integrated intensity of these high-frequency bands could be treated as semi-quantitative evaluating the relative amount of specific borate groups in glasses. The fraction of four-coordinated boron atom, N_4, could be estimated using the relationship:

$$N_4 = \frac{I_{p3}}{\sum_{i=1}^{4} I_{Pi} + I_{p3}} \quad (1)$$

where I_{Pi} represents the integrated intensity of P_i band obtained from the deconvoluted results. Using eqn (1), the value of N_4 in glasses was estimated and a linear decrease was found along with the MoO_3 concentration (Fig. 4).

Raman spectra of Li_2O–B_2O_3–MoO_3 high-temperature solutions

Raman spectra of LBM1–6 solutions were obtained at high temperature 50 K above the crystallization points, and the spectra fitting was performed carefully with the similar models of the glassy samples (Fig. 5). At high temperatures, Raman peaks broaden and shifted to lower wavenumbers due to the thermal broadening and expansion of the structures. The symmetric stretching vibrations peak of isolated MoO_4 tetrahedrons was observed a shift from 955 cm^{-1} in glasses to 937 cm^{-1} in high-temperature solutions, and the Raman peak ascribed to Mo=O bonds of MoO_6 octahedrons shifting from 973 to 960 cm^{-1}. When the MoO_3 content increased, high-temperature Raman spectra of solutions showed a similar evolution tendency with that of glasses, except for LBM6. Using $Li_2O{\cdot}3MoO_3$ as the flux, the LBM6 solution showed a drastic change of Raman spectrum (Fig. 5 LBM6). Despite a high MoO_3 content, the strongest Raman peak for LBM6 is at 937 cm^{-1}, which was ascribed to MoO_4 tetrahedrons. The weaker intensity of 960 cm^{-1} indicated

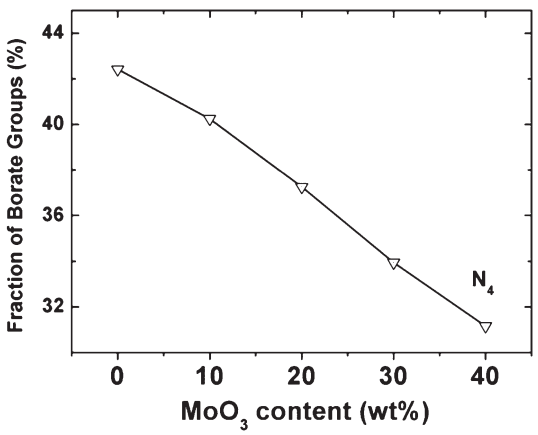

Fig. 4 Fraction of the four-coordinated boron atoms against MoO_3 content.

Table 2 Peak parameters of four components for the high-frequency bands

	P_1			P_2			P_3			P_4		
Sample	Peak (cm^{-1})	FWHM (cm^{-1})	NII[a] (a.u.)	Peak (cm^{-1})	FWHM (cm^{-1})	NII (a.u.)	Peak (cm^{-1})	FWHM (cm^{-1})	NII (a.u.)	Peak (cm^{-1})	FWHM (cm^{-1})	NII (a.u.)
LBM0	1262	69	4.3	1352	95	16.7	1454	136	73.7	1534	51	5.3
LBM1	1249	60	5.1	1338	124	23.9	1457	147	67.4	1537	55	3.6
LBM2	1244	74	11.1	1336	101	22.4	1452	138	59.4	1535	57	7.1
LBM3	1253	74	9.7	1345	130	34.4	1465	131	51.4	1539	53	4.6
LBM4	1252	70	9.6	1346	140	41.2	1470	129	45.3	1539	40	3.9

[a] NII = Normal Integrated Intensity.

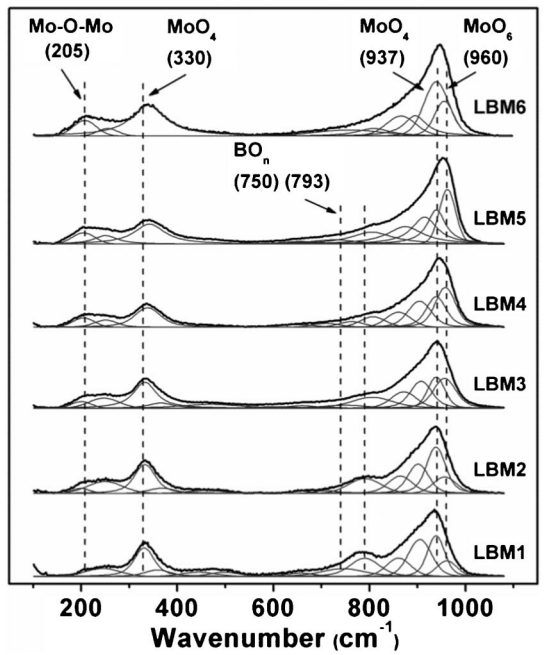

Fig. 5 Experimental Raman spectra and the fitting results of LBM1–6 solutions.

the addition of Li_2O led to the reduction of MoO_6 octahedrons in high-temperature solution.

^{11}B MAS NMR spectra of Li_2O–B_2O_3–MoO_3 glasses

^{11}B MAS NMR spectra of borate glasses with different MoO_3 contents are shown in Fig. 6 with curve simulation using three bands ascribed to the $BØ_4$ tetrahedron, the $BØ_3$ triangle in network and in boroxol rings, respectively. The parameters of these bands are obtained and listed in Table 3. For all investigated glasses, the strongest peak with the isotropic chemical shift δ_{iso} = 0.4–0.6 ppm was ascribed to the four-coordinated boron atom in $BØ_4$ tetrahedrons,[21,23,35] whose chemical shifts were observed to increase slightly as the MoO_3 content increased (Fig. 6). The chemical shifts of two types of $BØ_3$ triangles remained constant: the one in network was about ~14.00 ppm; the other in boroxol rings was about ~18.00 ppm.[36] The fractions of these boron oxide species in glasses obtained from MAS NMR data (Fig. 7) were consistent with those estimated from high-frequency Raman spectra (Fig. 4). The LBM0 glass had the highest fraction value of 40% for the $BØ_4$ tetrahedron. When the MoO_3 content increased, the value linearly decreased to 31% for the LBM4, on the contrary, the fraction of $BØ_3$ triangles in boroxol rings, N'_3, increased. These consistent results obtained from the independent MAS NMR experiment not only suggest that the Raman spectra deconvolutions performed in this work are reliable, but also indicate that $BØ_4$ tetrahedrons transform into $BØ_3$ triangles in boroxol rings along with the MoO_3 content increases in glasses.

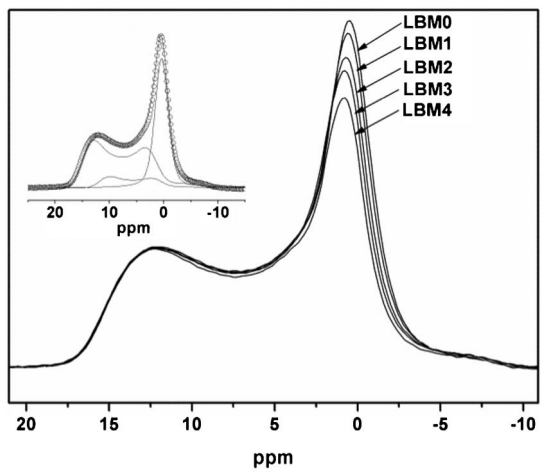

Fig. 6 Experimental ^{11}B MAS NMR spectra of LBM0–4 borate glasses (solid line). Inset shows the curve-fitting of LBM0 as an example.

Discussion

Molybdenum, boron and lithium environment in Li_2O–B_2O_3–MoO_3 ternary glasses

In the Li_2O–B_2O_3 binary glasses, three- and four-coordinated boron oxide species are the basic structural formers in the form of $BØ_3$ planar triangles and $BØ_4$ tetrahedrons, respectively. With the introduction of Li_2O into the pure B_2O_3, the electrically neutral $BØ_3$ triangles transform into the negatively charged $BØ_4$ tetrahedrons. On the other hand, lithium cations locate at the charge compensator positions to provide the local charge neutrality, which have two distinct sites near the negatively charged $BØ_4$ tetrahedrons and non-bridging oxygen bonds (NBO), respectively.[37–39]

Spectroscopic investigations have suggested that molybdenum ions are present in two valence states Mo(VI) and Mo(V) in borate glasses, which locate in tetrahedral sites for the MoO_4 and in octahedral sites for the distorted MoO_6, respectively.[40–42] When the MoO_3 content is low, the predominant molybdenum oxides species are MoO_4 tetrahedrons (Fig. 2). As the MoO_3 content increases, the amount of MoO_6 octahedrons increases gradually. Compared with the borate glass without MoO_3, the addition of molybdenum oxide could effectively change the relative amounts of various borate oxides species in glasses. When the MoO_3 content increases, a linear concentration decrease of $BØ_4$ tetrahedrons is observed by ^{11}B MAS NMR as well as Raman spectra (Fig. 4 and 7).

Concerning the activities of lithium ions, the simple bond valence model could help to understand the structural characteristics and evolution tendencies of Li_2O–B_2O_3–MoO_3 glasses with composition. According the Pauling's second rule, the sum of the bond valence S_{ij} around the atom is equal to the theoretical oxidation states V_i. The theoretical value V_i of an oxygen atom is about 2.0 $\pm$ 0.1 valence units, and the sum of bond valence for oxygen atom should not exceed this value. Because the bond valence S_{ij} between atom i and j has the semi-empirical relationship with the bond length d_{ij}:[43]

$$S_{ij} = \exp[(R_{ij} - d_{ij})/0.37] \quad (2)$$

Table 3 ^{11}B MAS NMR parameters of three- and four-coordinated boron sites in glasses, where δ is the isotropic chemical shift, CQ is the quadrupole coupling constant, η is the asymmetry parameter and $N_{3/4}$ is the fraction of three- or four-coordinated boron

	BO_3 sites[a]				BO'_3 sites[b]				BO_4 sites		
Example	δ/ppm	CQ/MHz	η	N_3%	δ/ppm	CQ/MHz	η	N_3%	δ/ppm	χ	N_4%
LBM0	14.06	2.34	0.03	10.41	17.08	2.57	0.14	50.26	0.40	2.88	39.33
LBM1	14.04	2.34	0.03	11.53	18.08	2.57	0.14	51.70	0.43	2.66	36.77
LBM2	13.91	2.34	0.03	11.06	18.01	2.57	0.14	54.26	0.49	2.56	34.69
LBM3	13.92	2.34	0.03	10.90	18.01	2.57	0.14	55.81	0.59	2.56	33.29
LBM4	14.11	2.34	0.03	11.15	18.14	2.57	0.14	58.20	0.60	2.06	30.64

[a] The $B\emptyset_3$ triangles in network. [b] The $B\emptyset_3$ triangles in boroxol rings.

for Mo–O bonds, the bond valence parameter R_{ij} is 1.908 Å,[44] and the average d_{Mo-O} obtained by Mo K-edge EXAFS data[45–47] is about 1.76–1.78 Å. Therefore, the bond valence S_{Mo-O} in MoO_4 tetrahedrons is estimated to be 1.41–1.49 v.u. This value is so high that the Mo–O bonds in tetrahedrons cannot connect with any type of bridging oxygen. In boron oxides species, the ideal bond valence of B–O bonds is 1 v.u. in a $B\emptyset_3$ triangle and 0.75 v.u. in a $B\emptyset_4$ tetrahedron. If a bridging oxygen atom connected with Mo and B ions, the sum of the bond valences will exceed 2.0 $\pm$ 0.1 v.u. Therefore, MoO_4 tetrahedrons have to be isolated in borate glasses, which cannot connect with the borate network. This may explain why no Raman peaks ascribed to Mo–O–B bonds are observed in glass spectra.

Due to the negative charge of the isolated MoO_4 tetrahedrons, the charge compensation of these species could be achieved by lithium ions. These lithium ions initially charge compensated to $B\emptyset_4$ tetrahedrons in the borate parent glass. Without lithium ions for charge compensation, $B\emptyset_4$ tetrahedrons become unstable, and then transform into the electrically neutral $B\emptyset_3$ triangles. The process is represented as:

$$MoO_3 + 2(B\emptyset_4^- + Li^{+(comp)}) \Leftrightarrow (MoO_4^{2-} + 2Li^{+(mod)}) + 2B\emptyset_3 \quad (3)$$

On the other hand, the isomerization reaction (eqn (3)) also suggests that the local environments of lithium ions would be changed during this process. Initially, Li^+ in borate glasses preferentially locates in charge compensating sites around the $B\emptyset_4$ tetrahedrons, as the addition of molybdenum oxide, proportions of lithium ions transfer to the network modifying site near NBOs of the MoO_4 tetrahedrons. The strong interaction between lithium ions and NBOs shortens lithium–oxygen bonds effectively, and results in the reduction of the coordination numbers of lithium ions. In the present work, this transformation was proven by the MoO_3-dependent ^{7}Li MAS NMR. For the central isotropic peak of ^{7}Li, a subtle shift to lower frequency was observed as the MoO_3 increases (Fig. 8). A similar result has been obtained from the MAS NMR investigation of alkali borate glasses,[24] and was ascribed to the coordination environment change of the network-modifying alkali cations (Li, Na, K, Rb, Cs) in glasses.

Because molybdenum atoms are introduced into the borate glasses as MoO_3, each molybdenum atom is surrounded by three NBOs, however, in glasses, molybdenum atoms locate in four-coordinated tetrahedral sites with four NBOs. Thus each introduced molybdenum atom needs at least one more NBO obtained from the borate parent network. It results in loss of oxygen atoms of the four-coordinated $B\emptyset_4$ tetrahedrons, and their transformation into three-coordinated $B\emptyset_3$ triangles. When the MoO_3 content increases gradually, the parent

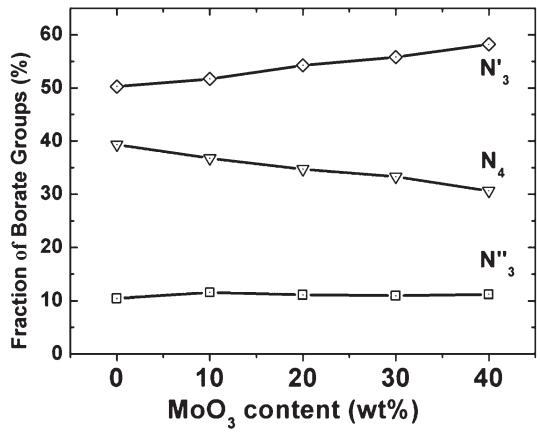

Fig. 7 Fraction of various boron oxides species against MoO_3 content; N_4 represents the $B\emptyset_4$ tetrahedron; N'_3 represents the $B\emptyset_3$ triangles in boroxol rings; N''_3 represents the $B\emptyset_3$ triangles in the network.

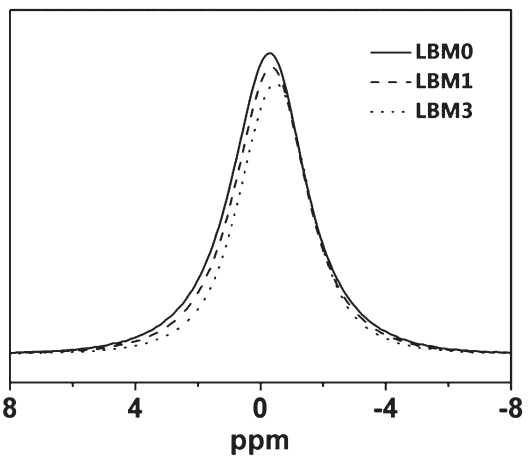

Fig. 8 ^{7}Li MAS NMR spectra of borate glasses with MoO_3.

network will be insufficient to satisfy the requirement of oxygen atoms. In order to adapt to the NBO shortage, Mo(VI) has to be reduced to Mo(V). Mo(V) ions locate at distorted octahedral sites, and moreover, the lower bond valence of Mo–O bonds in MoO_6 octahedrons makes it possible to bridge the oxygen atoms with other groups. Therefore, Raman spectra (Fig. 2) have indicated MoO_6 octahedrons increased with MoO_3 content increase, and the bending vibration of Mo–O–Mo at 210 cm^{-1} has suggested the bridging oxygen atom among MoO_6 octahedrons.

Structural characteristics of high-temperature solutions

High-temperature Raman spectra (Fig. 5) had proven that the structures and composition dependence of the high-temperature solutions were similar to those of their corresponding glasses. The original boron oxide units of the $Li_2O{\cdot}3B_2O_3$ melt were the cyclic species composed of $B\emptyset_4$ tetrahedrons and $B\emptyset_3$ triangles. With the addition of MoO_3, the tetrahedral and octahedral coordinated molybdenum oxide species were present in solutions, and an increase of MoO_6 octahedrons occurred along with the MoO_3 content; the boron oxide cyclic species did not change by the addition of molybdenum oxides, but the concentration of the $B\emptyset_4$ tetrahedrons decreased as the MoO_3 content increased.

Due to the weaker interaction with $B\emptyset_4$ tetrahedrons, the lithium charge compensators in borate glasses are easier to escape from their initial sites when the temperature increases. The temperature-induced site change of lithium ions decreases the stability of the $B\emptyset_4$ tetrahedrons, and causes the partial transformation of boron atoms from the $B\emptyset_4$ tetrahedrons to $B\emptyset_3$ triangles at high temperature. Neutron diffraction data[39] and MD simulations[48,49] proved the release of lithium ions from the charge compensating sites of the $B\emptyset_4$ tetrahedrons, and indicated the preferential association of lithium ions with NBOs in melts. Because the isolated MoO_4 tetrahedrons contain four NBOs, the availability of lithium cations will also promote the conversion of MoO_6 octahedrons to MoO_4 tetrahedrons at high temperature:

$$Mo\emptyset_6 + 2\left(B\emptyset_4^- + Li^{+(comp)}\right) \Leftrightarrow \left(MoO_4^{2-} + 2Li^{+(mod)}\right) + 2B\emptyset_3 \quad (4)$$

This isomerization reaction might explain why the relative Raman intensity of $B\emptyset_4$ and MoO_6 species for high-temperature solutions is lower than that for glasses. Moreover, the irregular Raman spectrum of the LBM6 solution, where the excess $Li_2O{\cdot}3MoO_3$ as the solvent, could be elucidated as follows: the addition of lithium oxides can provide not only the available lithium ions as the charge compensators but also the oxygen atoms as the NBOs, and result in the formation of a higher amount of MoO_4 tetrahedrons in the LBM6 solution.

The mechanism of flux-reduced LBO crystallization

The growth of crystals from the high-temperature solutions follows a kinetic process whereby the structural species in solution transform into the bulk nuclei, therefore, the structural information of solutions and bulk crystals is essential for understanding the crystal growth. The structural unit of LBO crystal is the triborate group $B_3\emptyset_7$, a six-membered ring containing two $B\emptyset_3$ triangles and one $B\emptyset_4$ tetrahedron. Four of seven bridging oxygen atoms in $B_3\emptyset_7$ rings are the terminal oxygen, which are shared by one $B\emptyset_3$ triangle and one $B\emptyset_4$ tetrahedron belonging to two neighboring rings. By sharing the terminal oxygen atoms, these $B_3\emptyset_7$ rings link together to form an infinite helical chain along the *c*-axis; these chains further connect with each other to form a three-dimensional network (Fig. 9). The average B–O bond lengths in the boron oxide triangle and tetrahedron are 1.371 and 1.476 Å, respectively, and the B–O bond strength in the $B\emptyset_4$ tetrahedron is weaker than that in the $B\emptyset_3$ triangle.[50] Our previous works[11–13] on the growth mechanism of the LBO crystal have revealed that the $B\emptyset_4$ tetrahedron played the role as the active connector in the boron oxide network, furthermore, the conversion of the $B\emptyset_3$ triangle to the $B\emptyset_4$ tetrahedron in the boundary layer is an important kinetic process for understanding the borate crystal growth. Considering this kinetic process and the melt structural information discussed above, the crystalline tendency of the $Li_2O{\cdot}3B_2O_3$ melt is $Li_2B_4O_7$ rather than LiB_3O_5 can be explained as follows.

For the borate crystallization with low lithium content, the formation of the $B\emptyset_4$ tetrahedron is essential for the borate oxide species transition from the short-range order in the liquid into the long-range order in the crystal. If a parent liquid has a high concentration of $B\emptyset_4$ tetrahedrons, on cooling, the crystallization of the solid phase containing a high $B\emptyset_4 : B\emptyset_3$ ratio is inevitable. In the above sections, Raman spectra have indicated that the primary borate oxide species in the $Li_2O{\cdot}3B_2O_3$ melt is a six-membered ring with one $B\emptyset_4$ tetrahedron. Although similar to the structural units of the LBO crystal, these rings would be polymerized by the formation of new $B\emptyset_4$ tetrahedrons in the boundary layer. The polymerization process will increase the ratio of $B\emptyset_4 : B\emptyset_3$ in the ring and results in the crystallization of the $Li_2B_4O_7$ phase, whose structural unit is a diborate group $B_4\emptyset_9$ composed of two $B\emptyset_3$ triangles and two $B\emptyset_4$ tetrahedrons (Fig. 10). Obviously, the ratio of $B\emptyset_4 : B\emptyset_3$ for $Li_2B_4O_7$ is 1 : 1 and hence higher than 1 : 2 for LBO, which implies that the

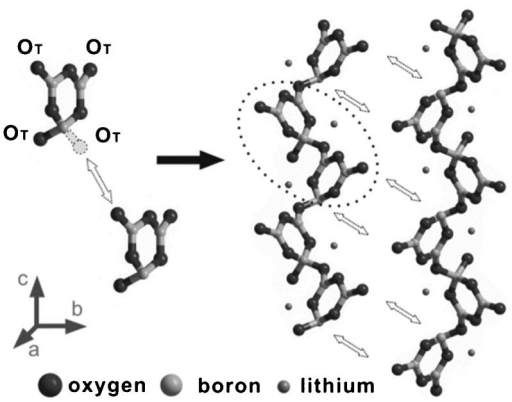

Fig. 9 Schematic of $B_3\emptyset_6$ rings bound together to form a $B_3\emptyset_7$ chain along the *c*-axis through the transition of $B\emptyset_3$ triangles into $B\emptyset_4$ tetrahedrons (left); the $B_3\emptyset_7$ chains bound together to form a three-dimensional network (right). O_T represents the terminal oxygen in $B_3\emptyset_7$ ring shared by one $B\emptyset_3$ triangle and one $B\emptyset_4$ tetrahedron belonging to two neighboring rings.

Fig. 10 Schematic of $Li_2B_4O_7$ crystallization in $Li_2O{\cdot}3B_2O_3$ melt.

concentration of $BØ_4$ tetrahedrons in the $Li_2O{\cdot}3B_2O_3$ melt is too high to crystallize the LBO phase.

Therefore, one effective way to induce the LBO growth is to reduce the concentration of $BØ_4$ tetrahedrons in high-temperature solutions. The above discussions have suggested that the addition of the MoO_3 flux could effectively reduce the amount of $BØ_4$ tetrahedrons in solutions. Due to high bond valence with oxygen, the molybdenum oxide species do not directly connect with the boron oxide network and prefer to be in the form of isolated MoO_4 tetrahedrons combining with lithium cations. As a consequence, the $BØ_4$ tetrahedron in the boron oxide ring becomes unstable without lithium ions for charge compensation, and then transitions into the $BØ_3$ triangle in boroxol, which causes the oxygen coordination of boron atoms to decrease in high-temperature solutions. These structural characteristics lead the crystallization of the solutions to the LBO phase, whose structure contains a low $BØ_4$: $BØ_3$ ratio.

On the other hand, the decrease of the concentration of $BØ_4$ tetrahedrons in high-temperature solutions can reduce the viscosity of the borate melts effectively. A low viscosity can enhance the atomic mobility in the solution, which is beneficial for the LiB_3O_5 crystal growth.[9,10] The nucleation and growth velocity of crystallization centers in such solution is promoted and as a consequence the growth of a large size crystal occurs.

Conclusions

In this work, we carried out a structural investigation of Li_2O–B_2O_3–MoO_3 glasses/high-temperature solutions using Raman spectra and ^{11}B, ^{7}Li solid-state NMR, and then discussed the correlation of the structures to LiB_3O_5 crystallization. The experimental data have revealed that: the primary boron oxide species of the $Li_2O{\cdot}3B_2O_3$ parent melt was the six-membered ring containing one $BØ_4$ tetrahedron; with the addition of MoO_3, molybdenum ions were present as the MoO_4 tetrahedron and the MoO_6 octahedron in solutions, which were not linked to the boron oxide network and preferred to be surrounded by lithium cations. The fraction of four-coordinated boron atoms, N_4, was found to exhibit a linear decrease along with the increase of MoO_3 content. Based on the structural information, the role of the MoO_3 flux in LiB_3O_5 crystallization might be understood in terms of an efficient reduction of $BØ_4$ tetrahedrons in the high-temperature solution, so that the crystallization tendency of the solution is toward the LiB_3O_5 crystal, whose structure contains a low $BØ_4$: $BØ_3$ ratio. This conclusion obtained in this work has an impact on understanding the role of the MoO_3 flux in the LiB_3O_5 crystal growth, and to optimize the crystal growth conditions in the future.

Acknowledgements

This work is financially supported by the National Natural Science Foundation of China (Grant No. 50932005, 51102239, 90922003 and 51172236).

References

1 C. Chen, Y. Wu, A. Jiang, B. Wu, G. You, R. Li and S. Lin, *J. Opt. Soc. Am. B*, 1989, **6**, 616–621.
2 D. N. Nikogosyan, *Appl. Phys. A: Solids Surf.*, 1994, **58**, 181–190.
3 D. P. Shumov, A. T. Nenov and D. D. Nihtianova, *J. Cryst. Growth*, 1996, **169**, 519–526.
4 H. G. Kima, J. K. Kang, S. H. Lee and S. J. Chung, *J. Cryst. Growth*, 1998, **187**, 455–462.
5 C. Parfeniuk, I. V. Samarasekera and F. Weinberg, *J. Cryst. Growth*, 1996, **158**, 514–522.
6 C. Parfeniuk, I. V. Samarasekera, F. Weinberg, J. Edel, K. Fjeldsted and B. Lent, *J. Cryst. Growth*, 1996, **158**, 523–533.
7 N. Pylneva, V. Kosyakov, A. Yurkin, G. Bazarova, V. Atuchin, A. Kolesnikov, E. Trukhanov and C. Zilling, *Cryst. Res. Technol.*, 2001, **36**, 1377–1384.
8 A. Kokh, N. Kononova, G. Mennerat, P. Villeval, S. Durst, D. Lupinski, V. Vlezko and K. Kokh, *J. Cryst. Growth*, 2010, **312**, 1774–1778.
9 Z. Hu, Y. Zhao, Y. Yue and X. Yu, *J. Cryst. Growth*, 2011, **335**, 133–137.
10 I. Nikolov, D. Perlov, S. Livneh, E. Sanchez, P. Czechowicz, V. Kondilenko and D. Loiacono, *J. Cryst. Growth*, 2011, **331**, 1–3.
11 D. Wang, S. Wan, S. Yin, Q. Zhang, J. You, G. Zhang and P. Fu, *CrystEngComm*, 2011, **13**, 5239–5242.
12 H. Min, Y. Jinglin, S. Patrick, Z. Guochun, W. Songming, W. Yuanyuan, J. Zifang, W. Lihong, F. Peizhen, W. Yicheng and Y. Shaotang, *CrystEngComm*, 2011, **13**, 3030–3034.
13 S. Wan, X. Zhang, S. Zhao, Q. Zhang, J. You, L. Lu, P. Fu, Y. Wu and S. Yin, *Cryst. Growth Des.*, 2008, **8**, 412–414.
14 S. Wan, B. Teng, X. Zhang, J. You, W. Zhou, Q. Zhang and S. Yin, *CrystEngComm*, 2010, **12**, 211–215.
15 S. Wan, X. Zhang, S. Zhao, Q. Zhang, J. You, H. Chen, G. Zhang and S. Yin, *J. Appl. Crystallogr.*, 2007, **40**, 725–729.
16 G. Calas, G. S. Henderson and J. F. Stebbins, *Elements*, 2006, **2**, 265–268.
17 D. P. Button, R. Tandon, C. King, M. H. Veléz, H. L. Tuller and D. R. Uhlmann, *J. Non-Cryst. Solids*, 1982, **49**, 129–142.
18 W. L. Konijnendijk and J. M. Stevels, *J. Non-Cryst. Solids*, 1975, **18**, 307–331.
19 E. I. Kamitsos and G. D. Chryssikos, *J. Mol. Struct.*, 1991, **247**, 1–16.

20 B. N. Meera and J. Ramakrishna, *J. Non-Cryst. Solids*, 1993, **159**, 1–21.
21 L. Züchner, J. C. C. Chan, W. Müller-Warmuth and H. Eckert, *J. Phys. Chem. B*, 1998, **102**, 4495–4506.
22 L.-S. Du and J. F. Stebbins, *J. Non-Cryst. Solids*, 2003, **315**, 239–255.
23 R. Martens and W. Müller-Warmuth, *J. Non-Cryst. Solids*, 2000, **265**, 167–175.
24 V. K. Michaelis, P. M. Aguiar and S. Kroeker, *J. Non-Cryst. Solids*, 2007, **353**, 2582–2590.
25 D. Massiot, F. Fayon, M. Capron, I. King, S. Le Calvé, B. Alonso, J.-O. Durand, B. Bujoli, Z. Gan and G. Hoatson, *Magn. Reson. Chem.*, 2002, **40**, 70–76.
26 B. P. Dwivedi and B. N. Khanna, *J. Phys. Chem. Solids*, 1995, **56**, 39–49.
27 A. K. Hassan, L. M. Torell, L. Börjesson and H. Doweidar, *Phys. Rev. B: Condens. Matter*, 1992, **45**, 12797–12805.
28 C. C. Williams, J. G. Ekerdt, J. M. Jehng, F. D. Hardcastle and I. E. Wachs, *J. Phys. Chem.*, 1991, **95**, 8791–8797.
29 C. C. Williams, J. G. Ekerdt, J. M. Jehng, F. D. Hardcastle, A. M. Turek and I. E. Wachs, *J. Phys. Chem.*, 1991, **95**, 8781–8791.
30 H. Hu and I. E. Wachs, *J. Phys. Chem.*, 1995, **99**, 10911–10922.
31 H. Hu, I. E. Wachs and S. R. Bare, *J. Phys. Chem.*, 1995, **99**, 10897–10910.
32 L. Seguin, M. Figlarz, R. Cavagnat and J. C. Lassègues, *Spectrochim. Acta, Part A*, 1995, **51**, 1323–1344.
33 A. Osipov and L. Osipova, *Glass Phys. Chem.*, 2009, **35**, 121–131.
34 T. Yano, N. Kunimine, S. Shibata and M. Yamane, *J. Non-Cryst. Solids*, 2003, **321**, 137–146.
35 L. van Wüllen, W. Müller-Warmuth, D. Papageorgiou and H. J. Pentinghaus, *J. Non-Cryst. Solids*, 1994, **171**, 53–67.
36 S. Kroeker and J. F. Stebbins, *Inorg. Chem.*, 2001, **40**, 6239–6246.
37 O. Majérus, L. Cormier, G. Calas and B. Beuneu, *Phys. Rev. B: Condens. Matter*, 2003, **67**, 024210.
38 L. Cormier, O. Majérus, D. R. Neuville and G. Calas, *J. Am. Ceram. Soc.*, 2006, **89**, 13–19.
39 G. D. Chryssikos, E. I. Kamitsos and M. A. Karakassides, *Phys. Chem. Glasses*, 1990, **31**, 109–116.
40 K. C. Radha, R. V. Anavekar, J. L. Rao and R. P. S. Chakradhar, *Appl. Magn. Reson.*, 2008, **35**, 1–13.
41 J. Maaß, H. Ahrens, P. Fröbel, K. Bärner, E. R. Giessinger and R. Braunstein, *Solid State Commun.*, 1993, **87**, 567–572.
42 S. Simon and Al. Nicula, *J. Non-Cryst. Solids*, 1983, **57**, 23–39.
43 F. D. Hardcastle and I. E. Wachs, *J. Raman Spectrosc.*, 1990, **21**, 683–691.
44 M. O'Keefe and N. E. Brese, *J. Am. Chem. Soc.*, 1991, **113**, 3226–3229.
45 G. Calas, M. Le Grand, L. Galoisy and D. Ghaleb, *J. Nucl. Mater.*, 2003, **322**, 15–20.
46 R. J. Short, R. J. Hand, N. C. Hyatt and G. Möbus, *J. Nucl. Mater.*, 2005, **340**, 179–186.
47 F. Farges, R. Siewert, G. E. Brown, A. Guesdon and G. Morin, *Can. Mineral.*, 2006, **44**, 731–753.
48 C.-P. E. Varsamis, A. Vegiri and E. I. Kamitsos, *Phys. Rev. B: Condens. Matter*, 2002, **65**, 104203.
49 A. Vegiri, C. P. E. Varsamis and E. I. Kamitsos, *Phys. Rev. B: Condens. Matter Mater. Phys.*, 2009, **80**, 184202.
50 J. Li, C.-G. Duan, Z.-Q. Gu and D.-S. Wang, *Phys. Rev. B: Condens. Matter*, 1998, **57**, 6925–6932.

